

Nonlinear Metasurface for Simultaneous Control of Spin and Orbital Angular Momentum in Second Harmonic Generation

Guixin Li,^{*,†, } Lin Wu,[‡] King F. Li,[†] Shumei Chen,[○] Christian Schlickriede,^{||} Zhengji Xu,^{‡,§} Siya Huang,[†] Wendi Li,^{†,⊥} Yanjun Liu,[#] Edwin Y. B. Pun,[∇] Thomas Zentgraf,^{||,§} Kok W. Cheah,[§] Yu Luo,^{*,‡,§} and Shuang Zhang^{*,○,§}

[†]Department of Materials Science and Engineering, Southern University of Science and Technology, Shenzhen, 518055, China

[&]Institute for Quantum Science and Engineering, Southern University of Science and Technology, Shenzhen, 518055, China

[‡]School of Electrical and Electronic Engineering College of Engineering, Nanyang Technological University, Singapore 639798

[§]Department of Physics, Hong Kong Baptist University, Kowloon Tong, Hong Kong

^{||}Department of Physics, University of Paderborn, Warburger Straße 100, D-33098 Paderborn, Germany

[⊥]Department of Mechanical Engineering, The University of Hong Kong, Pokfulam, Hong Kong, China

[#]Department of Electrical and Electronic Engineering, Southern University of Science and Technology, Shenzhen, 518055, China

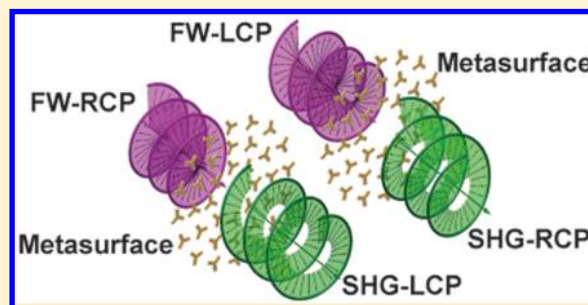
[∇]Department of Electronic Engineering and State Key Laboratory of Millimeter Waves, City University of Hong Kong, 83 Tat Chee Ave, Hong Kong

[○]School of Physics and Astronomy, University of Birmingham, Birmingham, B15 2TT, United Kingdom

Supporting Information

ABSTRACT: The spin and orbital angular momentum (SAM and OAM) of light is providing a new gateway toward high capacity and robust optical communications. While the generation of light with angular momentum is well studied in linear optics, its further integration into nonlinear optical devices will open new avenues for increasing the capacity of optical communications through additional information channels at new frequencies. However, it has been challenging to manipulate the both SAM and OAM of nonlinear signals in harmonic generation processes with conventional nonlinear materials. Here, we report the generation of spin-controlled OAM of light in harmonic generations by using ultrathin photonic metasurfaces. The spin manipulation of OAM mode of harmonic waves is experimentally verified by using second harmonic generation (SHG) from gold meta-atom with 3-fold rotational symmetry. By introducing nonlinear phase singularity into the metasurface devices, we successfully generate and measure the topological charges of spin-controlled OAM mode of SHG through an on-chip metasurface interferometer. The nonlinear photonic metasurface proposed in this work not only opens new avenues for manipulating the OAM of nonlinear optical signals but also benefits the understanding of the nonlinear spin-orbit interaction of light in nanoscale devices.

KEYWORDS: Metasurface, plasmonics, spin angular momentum, orbital angular momentum, second harmonic generation, optical vortex



The angular momentum of light has two freedoms, that is, spin and orbital (SAM and OAM). SAM of light is associated with circular polarizations; in comparison, light with OAM has a helical phase front characterized by $\exp(il\varphi)$, where l and φ are the topological charge and azimuthal angle, respectively.^{1,2} The unbounded topological charge of OAM provides infinite freedom for encoding light information. The combination of SAM and OAM of light promises great potentials for both classical and quantum communications.^{2–7} Conventional optical components such as q-plates and spatial light modulators have been extensively used to couple SAM with OAM together.^{8,9} However, the diffraction effects of conventional devices inevitably limit the on-chip integration of

optical functionalities, which are important for ultrahigh capacity information processing. The fast development of photonic metamaterials^{10–13} and metasurfaces^{14–32} offers new solutions to circumvent these constraints. Light-matter interactions can be manipulated by using subwavelength meta-atoms thereby enabling the realization of various extraordinary optical functions. While the fabrication of the three-dimensional metamaterial operating in optical regime is

Received: October 19, 2017

Revised: November 13, 2017

Published: November 16, 2017

difficult, the advent of two-dimensional metasurfaces greatly eases this challenge.^{14–32} In linear optics, photonic metasurfaces, consisting of Pancharatnam–Berry (P-B) phase elements,^{30–35} have been employed in numerous studies to realize flat-lens imaging,^{19,30} optical spin Hall effect,^{20,21} high efficiency holography,^{27,28} and so on. Recently, the optical spin-controlled metasurfaces have received considerable interest since they have intrinsic advantages to simultaneously control the SAM and OAM of light.^{21,23,24,31,32,35} Importantly, by simply changing the in-plane orientation angle of the spin-active meta-atom, the scattered light from each meta-atom experiences a phase twice its orientation angle, proving a full phase range from zero to 2π . Moreover, the pixel size of metasurface is at the subwavelength scale, thus eliminating the higher order diffraction that is undesirable in many applications. Both the subwavelength pixel size and the capability of continuous phase manipulation endow the spin-controlled metasurface with many advantages superior to that of conventional diffractive optical elements.^{20,27,28,30–32}

In nonlinear optics, there have been growing interests in manipulating both SAM^{36–41} and OAM^{42–46} of light. One strategy is to use plasmonic metasurfaces where circularly polarized harmonic generations follow similar selection rules as those in optical crystals.^{37,38} For instance, when illuminated by circularly polarized fundamental waves (FW) along the rotational axis, a meta-atom with m -fold rotational symmetry only allows harmonic generation orders of $n = jm \pm 1$, where j is an arbitrary integer and the \pm sign corresponds to harmonic generations with the same and opposite spins as the FW, respectively. Later, it was verified that the nonlinear polarizabilities of the meta-atom can be expressed as $p_{\theta,\sigma,\sigma}^{no} \propto e^{(n-1)i\sigma\theta}$ and $p_{\theta,-\sigma,\sigma}^{no} \propto e^{(n+1)i\sigma\theta}$ for harmonic generations. Here, $\sigma = \pm 1$ represents the same and opposite spins as those of the FW, respectively; θ is the in-plane orientation angle of the meta-atom.³⁹ Similar to the definition of a geometric P-B phase element in the linear optics, the phase factors: $(n - 1)\sigma\theta$ and $(n + 1)\sigma\theta$ for harmonic generations can be defined as the nonlinear P-B phase, which depends only on the orientation angle of the meta-atoms. Therefore, third harmonic generation (THG) from plasmonic meta-atoms with 4-fold rotational symmetry has an opposite SAM as compared to that of FW and experiences a phase factor of $4\sigma\theta$.³⁹ In comparison, the meta-atom with one-fold rotational symmetry, such as split ring resonator, has two different nonlinear P-B phases ($\sigma\theta$ and $3\sigma\theta$) for the second harmonic generation (SHG) with different SAM states.^{40,41}

On the other hand, two methods for generating OAM for harmonic signals are commonly used in nonlinear optical processes. The first one makes use of the conservation principle of angular momentum, where the high-harmonic wave inherits the OAM from the FW. For instance, the FW has a topological charge of l_0 gives rise to an OAM of nl_0 for the n th harmonic generations.⁴² However, this method cannot be applied to high harmonic generations in gas medium, where the conservation law of OAM fails.⁴³ The second approach to generate OAM mode for high harmonic generations directly introduces phase singularity with topological charge of q into the nonlinear media. For example, the electric poling technique was used to realize Fork-type binary phase modulation (0 and π) in nonlinear crystals for the SHG process.⁴⁴ In this case, the SHG wave has a topological charge l of OAM equal to $2l_0 + q$. However, the pitch size of phase pattern in the poled crystal is usually at the scale of tens of microns, which is much larger

than the wavelength of SHG wave, and therefore inevitably introduces multiple diffraction orders of SHG. Alternatively, OAM of SHG and THG waves be generated via an ultrathin Fork-type microstructure.⁴⁵ More recently, OAM mode of SHG was also successfully realized on a Fork-type metasurface consisting of U-shaped meta-atoms with subwavelength pixel size and binary phase modulation.⁴⁶ However, this kind of meta-atom does not have high order rotational symmetry ($m \geq 3$), which is difficult to allow the manipulation of SAM state of SHG wave.

To the best of our knowledge, all the previous works on angular momentum of light in nonlinear optics deal with either SAM or that of OAM.^{42–46} None of them provide a systematic study on how the SAM and OAM interact with each other in the nonlinear process. Here, we propose a metasurface based approach to simultaneously manipulate both SAM and OAM of light in harmonic generations. The OAM information on harmonic generations with various topological charges can be encoded into the nonlinear photonic metasurface. The orientation angle of the meta-atoms is defined by $q\theta(x, y)$, where $\theta(x, y) = \arctan(y/x)$; q is the topological charge of metasurface; x and y are the coordinate axes.³⁵ For a FW with a SAM state of σ , the n th harmonic generations from the nonlinear photonic metasurface acquire a SAM state of $s = \pm\sigma$ and an OAM state of $l = (n \mp 1)\sigma q$ owing to the nonlinear spin–orbital interaction. Instead of using the binary phase modulation, here we adopt a continuous control of nonlinearity as it helps eliminate the issue of multiple diffraction orders for the generated nonlinear signal. Although the continuous control of nonlinearity phase can be realized by appropriately designing the aspect ratio of gold nanoapertures⁴⁷ or changing the orientation angle of U-shaped meta-atom,^{40,41,48} the magnitude of the nonlinear signal from individual nanoaperture and U-shaped meta-atom is highly sensitive to the polarizations of the FW. This problem limits the design of nonlinear optical functionalities. In comparison, the amplitude of harmonic generations from meta-atoms with high-order rotational symmetries is robust to the FW with circular polarizations, and only the nonlinear P-B phase varies with different orientation angles. Therefore, the SAM states of both FW and harmonic generations are maintained when they propagate along the rotational axis of the metasurface.

Design of Nonlinear Metasurface. To realize simultaneous control of both SAM and OAM in harmonic generations, here we study the SHG from nonlinear metasurface consisting of gold meta-atom with 3-fold (C3) rotational symmetry (Figure 1). From the selection rules of harmonic generations with circularly polarized FW, only SHG with opposite SAM state to that of FW is allowed and the nonlinear P-B phase of each C3 meta-atom is $3\sigma\theta$, where θ is the in-plane orientation angle of the meta-atom.^{39,49,50} Figure 2a–c shows the local phase distributions of SHG for nonlinear C3 metasurfaces with $q = 1/3, 2/3$, and 1. The states of spin and orbital angular momenta of SHG from the C3 metasurface are $s = -\sigma$ and $l = 3\sigma q$, respectively. The topological charges of OAM associated with of the circularly polarized SHG generated by these metasurfaces should be equal to $l = 1, 2$, and 3 respectively. To experimentally verify the above assumptions, three plasmonic metasurfaces consisting of gold C3 meta-atoms are fabricated on ITO coated glass substrate using standard electron beam lithography technique (Figure 2d–f). The linear optical properties of these three metasurfaces are characterized using a Fourier transformation infrared spectrometer. We found that

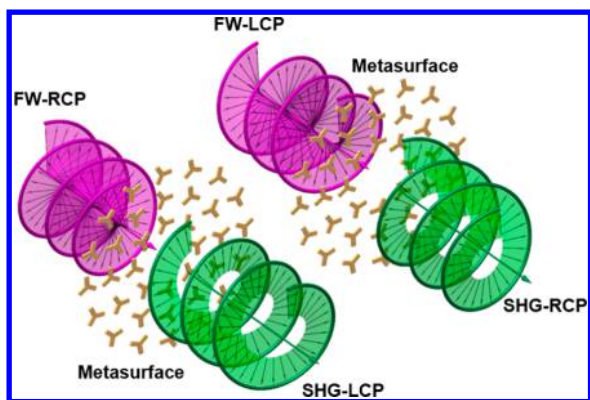


Figure 1. Schematic of spin controlled generation of OAM of SHG by using nonlinear photonic metasurface. The metasurface consists of C3 plasmonic meta-atoms with 3-fold symmetry. For an FW with two spin states (LCP and RCP) normally incident onto the nonlinear photonic metasurface with C3 symmetry, generation of SHG waves with opposite handedness to that of FW are allowed. By encoding the phase singularity into the metasurfaces, the SHG vortex beams with spin-controlled topological charges are generated.

the measured transmission spectra agree well with calculated results (Figure 2g,h). The resonant dips at the wavelength of $\lambda \sim 1060$ nm in the transmission spectra correspond to localized plasmonic resonance of each C3 meta-atom.

Nonlinear Optical Experiment. In Figure 2h, the spectral-resolved SHG responses from the three metasurfaces (see Supporting Information) are numerically calculated. The strong field localization under plasmonic resonance conditions can be utilized to boost the nonlinear optical efficiency, an effect already demonstrated in previous research.^{37,39} It should be noted that the SHG signals mainly come from the nonlinearity of gold^{36,39,40,48} and 15 nm thick ITO layer mainly serves as a conductive layer for electron beam lithography and its contribution to SHG is negligible. The SHG from the C3 metasurface with $q = 1/3$ was characterized by using a femtosecond laser with tunable wavelength output. The circularly polarized fundamental wave (FW) is normally incident onto the metasurfaces after passing through an objective lens with NA = 0.1. The intensity of the SHG signals with left- and right-circular polarizations (LCP and RCP) can be measured by using a spectrometer with a photomultiplier tube detector. For FW at wavelength of 1060, 1100, 1140, and 1180 nm, we measured the spectral response of SHG (see

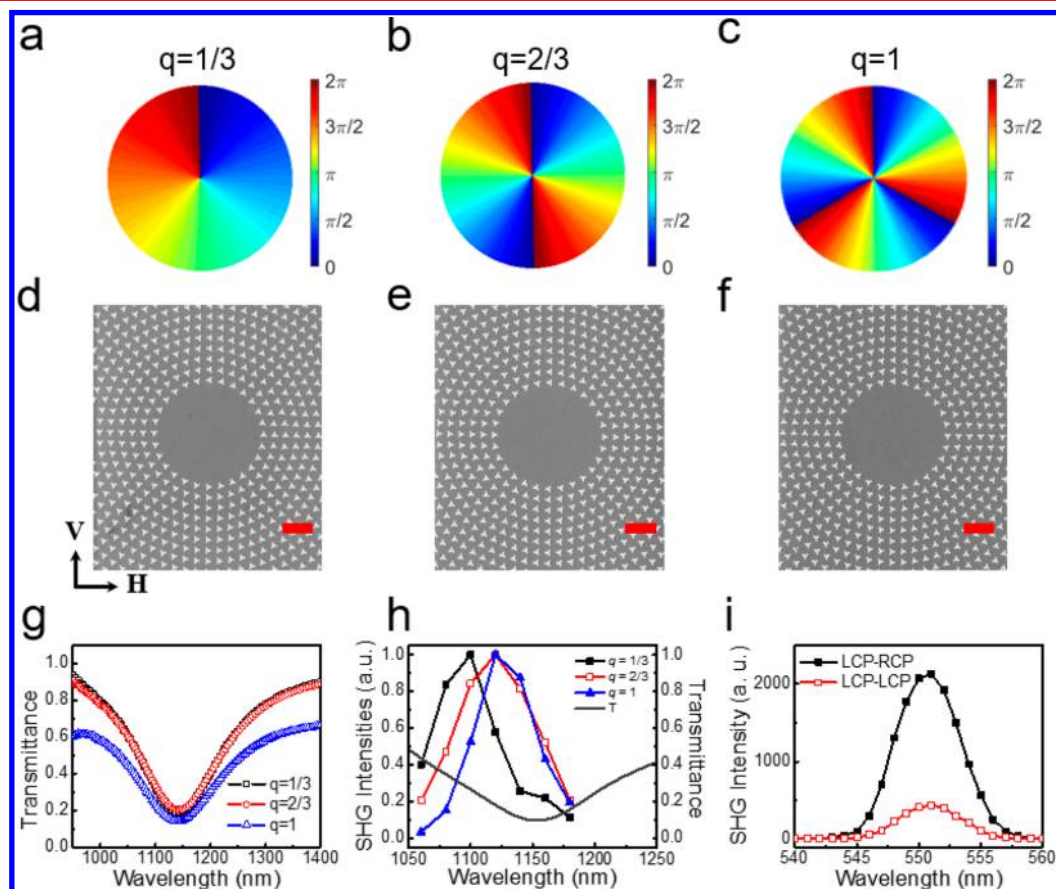


Figure 2. Design and optical properties of nonlinear photonic metasurface. (a–c), real space phase distribution of SHG from the nonlinear photonic metasurface with various phase singularities $Q = 1, 2,$ and 3 . (d–f), scanning electron microscope images of gold plasmonic metasurface with $q = 1/3, 2/3,$ and 1 . The gold meta-atom with C3 symmetry is fabricated on ITO-coated glass by using electron beam lithography and metal lift off process. The thickness of gold is 30 nm, scale bar: 600 nm. (g–i) Characterization of second harmonic generation from the nonlinear photonic metasurface. (g) Measured transmission spectra of photonic metasurfaces with $q = 1/3, 2/3,$ and 1 , the transmission dips represent the plasmonic resonant wavelengths. (h) Calculated SHG efficiency from the three kinds of metasurfaces for the circularly polarized FW. (i) Characteristics of SHG from nonlinear metasurface with $q = 1/3$. At wavelength of 1100 nm, the spectra of SHG with both same (LCP–LCP) and opposite polarization states (LCP–RCP) compared to that of the FW are measured. It can be found that the SHG_RCP signal is much stronger than SHG_LCP.

Supporting Information). The maximum efficiency of SHG appears at fundamental wavelength of 1100 nm, which agrees well with the calculation (Figure 2h). Figure 2h shows that SHG signal with the same SAM state as that of the FW (LCP–LCP) is much weaker than that with opposite SAM state (LCP–RCP). Ideally, the LCP–LCP component should be forbidden according to the selection rules of circularly polarized harmonic generations.^{37,38} However, due to the sample imperfection coming from the nanofabrication process, the C3 meta-atoms do not have perfect rotational C3 symmetry which is why we can observe the SHG for LCP–LCP measurement scheme. For the LCP–RCP measurement, the power dependence of SHG at wavelength of 550 nm has a slope value of 2.03, which agrees well with the theoretical value of 2.0 for SHG process (see Supporting Information). The absolute SHG conversion efficiency at wavelength of 550 nm is $\sim 4.51 \times 10^{-9}$.

Consequently, the far-field imaging of SHG radiations is characterized at the fundamental wavelength of 1100 nm for all the three metasurfaces. The SHG beams are collected by a second objective lens with NA = 0.3 with its Fourier plane imaged onto a charge coupled device camera after filtering out the FW by using band-pass filters (see Supporting Information). As shown in Figure 3, SHG beams with RCP SAM state have donut shapes while the ones with LCP state have very low

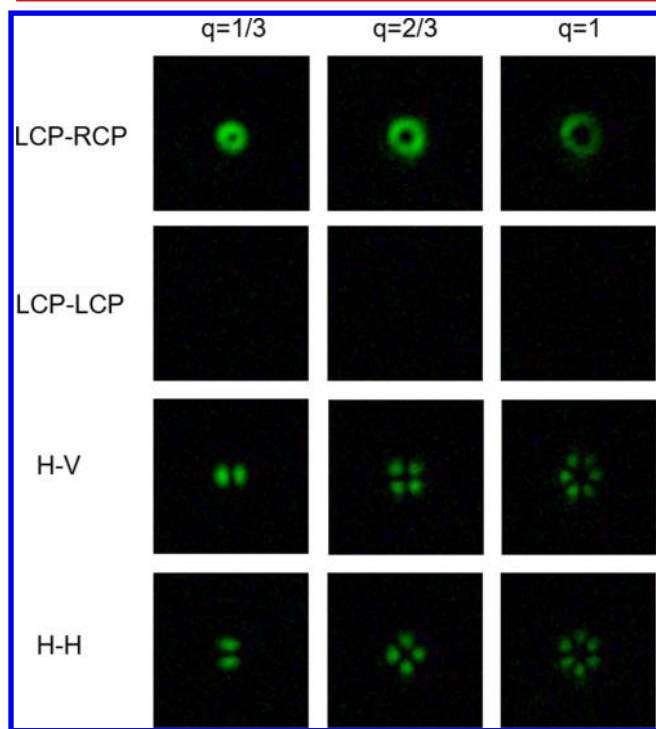


Figure 3. Measurement intensity distributions of SHG from metasurfaces with $q = 1/3, 2/3,$ and 1 . Under pumping of left circularly polarized FW, the SHG radiation with RCP- and LCP-components (first and second rows) are measured in the far field. For the LCP(FW)–RCP(SHG) measurement, SHG vortex beams with increasing radiuses are observed. In comparison, no obvious SHG signals are found for LCP(FW)–LCP(SHG) measurement. The third and fourth rows show the results for FW with horizontal polarization (H), the SHG signals with horizontal (H) and vertical (V) polarizations were recorded by using CCD camera. From the petal numbers of SHG interference pattern, the absolute value of the topological charge of SHG vortex can be identified.

intensity, which is close to the background noise. On the basis of our theoretical predictions, the donut beams of SHG at far field in Figure 3 are optical vortices with different topological charges. To quantify the topological charges associated with the OAM of SHG waves, the conventional method such as Mach–Zehnder interferometry is usually used. This technique involves both the spatial and temporal overlaps of optical signals from two arms of an interferometer, which is usually challenging for ultrafast laser beams. To circumvent this constraint, we proposed a different approach and used the coaxial metasurface interferometry. For linear polarized FW with both LCP and RCP components, the topological charge of SHG vortex beams radiated from the C3 nonlinear metasurfaces should be l and $-l$, respectively. The SAM states of the SHG vortexes are RCP and LCP, which are opposite to those of the FW. By choosing the linear polarized components from the two SHG vortexes, we are able to observe the interference patterns of the two counter-handed OAM modes with topological charge: $\pm l$. The interference pattern is expected to be the Hermite–Gaussian (HG) mode of light with a petal number of $2l$.⁹ In this way, one can quantify the topological charge of the OAM mode of SHG wave. As shown in third and fourth rows of Figure 3, the petal number of the HG modes for the three nonlinear metasurfaces equals to $2l = 2, 4,$ and 6 . Thus, we can experimentally retrieve the topological charge of the OAM of SHG vortexes with $l = \pm\sigma, \pm 2\sigma,$ and $\pm 3\sigma$. We also performed numerical calculations of the SHG radiations to verify our experimental observations.

Numerical Simulations of SHG on Metasurfaces.

Figure 4 shows the calculated results, in which the far field

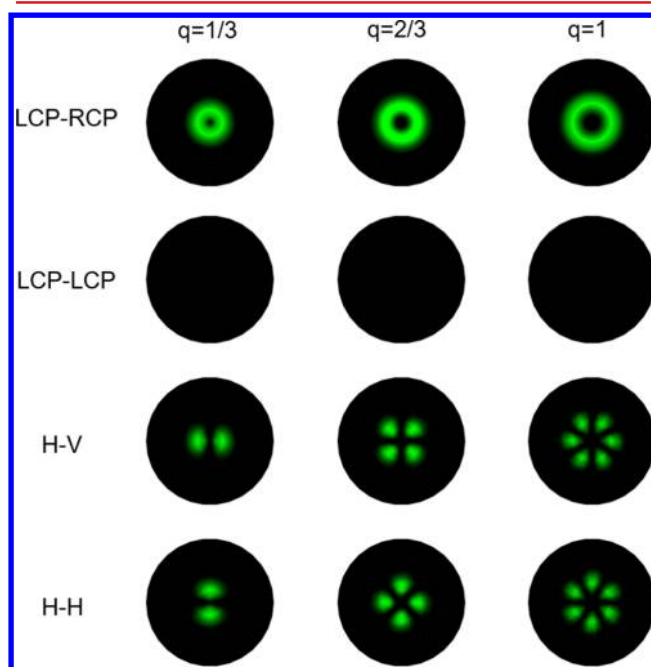


Figure 4. Calculated intensity distributions of SHG from metasurfaces with $q = 1/3, 2/3,$ and 1 . For FW with LCP state, the far field SHG radiation with RCP- and LCP- components (first and second rows) are plotted. In the first row, SHG vortex beams with increasing radius are observed. In comparison, SHG signals with LCP state cannot be obtained. For FW with horizontal polarization (H, $\alpha_0 = 0^\circ$), far field SHG signals with both H- ($\varphi = 0^\circ$) and vertical (V, $\varphi = 90^\circ$) polarizations are also calculated (third and fourth rows). It can be found that all the calculated results agree well with the experimental results in Figure 3.

radiation of the SHG from the metasurfaces for various polarizations of FW are summarized. In the calculation, we considered the SHG from 10 concentric rings in each of the three metasurfaces. For each C3 meta-atom, SHG with RCP and LCP states have relative nonlinear P-B phases of 3θ and -3θ , respectively. By integrating the right- and left- circularly polarized SHG in the far field, we observe donut beams with increasing radii for $q = 1/3, 2/3, 1$ (Figure 4). For the vertically polarized FW, the far field radiation pattern for horizontally (H-) and vertically (V-) polarized SHG have petal numbers of $6q$. It can be found that the numerical simulations agree well with experimental results. The polarization property of the SHG wave can also be understood using the analytical methods. Assuming the linear polarization of FW, which can be decomposed to LCP and RCP states, $|L\rangle$ and $|R\rangle$, has an orientation angle of α_0 with respect to x -axis, the electric field of SHG with RCP and LCP states are given by $|R\rangle e_0^{-i2\alpha} e^{i3q\theta}$ and $|L\rangle e_0^{i2\alpha} e^{-i3q\theta}$, where θ is the polar angle. Adding the two SAM states of SHG waves together, the total electric field of SHG from the metasurfaces is then described by a Jones

matrix: $E_{\text{SHG}} \sim \begin{pmatrix} \cos(3q\theta - 2\alpha_0) \\ \sin(3q\theta - 2\alpha_0) \end{pmatrix}$. Then we know that the

SHG beam has a donut shape with vector polarization distribution. As shown in third and fourth rows of Figure 4, the vector polarization distribution of SHG wave can be characterized using the linear analyzer with polarization angle of φ (H/V: 0 and 90°). In addition, the vector distribution of SHG vortex wave also depends on the topological charges of the plasmonic metasurfaces (see Figure S4). Moreover, the in-plane mode rotation of the HG beam can be arbitrarily controlled by rotating the polarization angles of both FW and SHG waves (see Supporting Information).

Conclusion. We have demonstrated a nonlinear metasurface for generating SHG signals carrying OAMs. Our work not only opens new avenues for increasing the freedom of SAM–OAM modes in harmonic generations by using geometric Berry phase controlled nonlinear metasurfaces but also demonstrates a new methodology to measure the SAM–OAM mode of nonlinear optical signals through on-chip metasurface interferometry. For the first time, we can simultaneously control both the spin and orbital angular momentum of light in nonlinear optical processes. Our findings are expected to benefit the understanding of physics behind the nonlinear spin–orbit interaction of light on nanoscale devices. The low SHG conversion efficiency from plasmonic metasurfaces could be greatly improved by combining metasurface with the semiconductor, conventional nonlinear optical crystals and so on. For example, the SHG efficiency could be improved by several orders by aligning the optical resonances of metasurfaces with intersub-band transitions of quantum wells.⁵¹ Mediated by the high sensitivity of the state-of-the-art photodetectors, nonlinear photonic metasurfaces, as a complementary alternative to conventional nonlinear optical crystals, may find the wide range applications in optical switching or frequency conversions.

■ ASSOCIATED CONTENT

Supporting Information

The Supporting Information is available free of charge on the ACS Publications website at DOI: 10.1021/acs.nanolett.7b04451.

Additional figures and table (PDF)

■ AUTHOR INFORMATION

Corresponding Authors

*E-mail: ligx@sustc.edu.cn.

*E-mail: luoyu@ntu.edu.sg.

*E-mail: s.zhang@bham.ac.uk.

ORCID

Guixin Li: 0000-0001-9689-8705

Zhengji Xu: 0000-0002-0265-6228

Wendi Li: 0000-0002-7005-2784

Thomas Zentgraf: 0000-0002-8662-1101

Yu Luo: 0000-0003-2925-682X

Shuang Zhang: 0000-0003-4556-2333

Author Contributions

The manuscript was written through contributions of all authors. All authors have given approval to the final version of the manuscript. G.L. and L.W. contributed equally.

Notes

The authors declare no competing financial interest.

■ ACKNOWLEDGMENTS

G.L. would like to thank the National Natural Science Foundation of China (Grant 11774145) and Natural Science Foundation of Shenzhen Innovation Committee (Grant JCYJ20170412153113701). L.W. and Y.L. are supported by Singapore Ministry of Education (MOE) under Grant MOE2015-T2-1-145 and National Research Foundation CRP Grant NRF2015NRF-CRP002-008. K.W. and E.P. are supported by Hong Kong Research Grant Council, Area of Excellence (AoE P-02/12). S.M. was supported by Marie Curie Individual Fellowship (Grant H2020-MSCA-IF-703803-Non-linearMeta). S.Z. is supported by the European Research Council Consolidator Grant (TOPOLOGICAL).

■ REFERENCES

- (1) Poynting, J. H. *Proc. R. Soc. London, Ser. A* **1909**, *82*, 560–567.
- (2) Allen, L.; Beijersbergen, M. W.; Spreeuw, R. J. C.; Woerdman, J. P. *Phys. Rev. A: At., Mol., Opt. Phys.* **1992**, *45*, 8185–8189.
- (3) Mair, A.; Vaziri, A.; Weihs, G.; Zeilinger, A. *Nature* **2001**, *412*, 313–316.
- (4) Wang, X. L.; Cai, X. D.; Su, Z. E.; Chen, M. C.; Wu, D.; Li, L.; Liu, N. L.; Lu, C. Y.; Pan, J. W. *Nature* **2015**, *518*, 516–519.
- (5) Nagali, E.; Sansoni, L.; Sciarrino, F.; De Martini, F.; Marrucci, L.; Piccirillo, B.; Karimi, E.; Santamato, E. *Nat. Photonics* **2009**, *3*, 720–723.
- (6) Leach, J.; Jack, B.; Romero, J.; Jha, A. K.; Yao, A. M.; Franke-Arnold, S.; Ireland, D. G.; Boyd, R. W.; Barnett, S. M.; Padgett, M. J. *Science* **2010**, *329*, 662–665.
- (7) Wang, J.; Yang, J. Y.; Fazal, I. M.; Ahmed, N.; Yan, Y.; Huang, H.; Ren, Y. X.; Yue, Y.; Dolinar, S.; Tur, M.; Willner, A. E. *Nat. Photonics* **2012**, *6*, 488–496.
- (8) Marrucci, L.; Manzo, C.; Paparo, D. *Phys. Rev. Lett.* **2006**, *96*, 060503.
- (9) Yao, M. A.; Padgett, M. J. *Adv. Opt. Photonics* **2011**, *3*, 161–204.
- (10) Soukoulis, C. M.; Wegener, M. *Nat. Photonics* **2011**, *5*, 523–530.
- (11) Hess, O.; Pendry, J. B.; Maier, S. A.; Oulton, R. F.; Hamm, J. M.; Tsakmakidis, K. L. *Nat. Mater.* **2012**, *11*, 573–584.
- (12) Zheludev, N. I.; Kivshar, Y. S. *Nat. Mater.* **2012**, *11*, 917–924.
- (13) Pendry, J. B.; Luo, Y.; Zhao, R. *Science* **2015**, *348*, 521–524.
- (14) Yu, N.; Genevet, P.; Kats, M. A.; Aieta, F.; Tetienne, J. P.; Capasso, F.; Gaburro, Z. *Science* **2011**, *334*, 333–337.
- (15) Kildishev, A. V.; Boltasseva, A.; Shalae, V. M. *Science* **2013**, *339*, 1232009.

- (16) Meinzer, N.; Barnes, W. L.; Hooper, I. R. *Nat. Photonics* **2014**, *8*, 889–898.
- (17) Yu, N.; Capasso, F. *Nat. Mater.* **2014**, *13*, 139–150.
- (18) Ni, X.; Emani, N. K.; Kildishev, A.; Boltasseva, V. A.; Shalae, V. *M. Science* **2012**, *335*, 427.
- (19) Sun, S.; He, Q.; Xiao, S.; Xu, Q.; Li, X.; Zhou, L. *Nat. Mater.* **2012**, *11*, 426–431.
- (20) Chen, X.; Huang, L. L.; Mühlenbernd, H.; Li, G. X.; Bai, B. F.; Tan, Q. F.; Jin, G. F.; Qiu, C. W.; Zhang, S.; Zentgraf, T. *Nat. Commun.* **2012**, *3*, 1198.
- (21) Li, G.; Kang, M.; Chen, S. M.; Zhang, S.; Pun, E. Y. B.; Cheah, K. W.; Li, J. S. *Nano Lett.* **2013**, *13*, 4148–4151.
- (22) Yin, X. B.; Ye, Z. L.; Rho, J.; Wang, Y.; Zhang, X. *Science* **2013**, *339*, 1405–1407.
- (23) Karimi, E.; Schulz, S. A.; De Leon, I.; Qassim, H.; Upham, J.; Boyd, R. W. *Light: Sci. Appl.* **2014**, *3*, e167.
- (24) Bouchard, F.; De Leon, I.; Schulz, S. A.; Upham, J.; Karimi, E.; Boyd, R. W. *Appl. Phys. Lett.* **2014**, *105*, 101905.
- (25) Lin, D.; Fan, P.; Hasman, E.; Brongersma, M. L. *Science* **2014**, *345*, 298.
- (26) Khorasaninejad, M.; Crozier, K. B. *Nat. Commun.* **2014**, *5*, 5386.
- (27) Zheng, G.; Mühlenbernd, H.; Kenney, M.; Li, G. X.; Zentgraf, T.; Zhang, S. *Nat. Nanotechnol.* **2015**, *10*, 308–312.
- (28) Arbabi, A.; Horie, Y.; Bagheri, M.; Faraon, A. *Nat. Nanotechnol.* **2015**, *10*, 937–943.
- (29) Aieta, F.; Kats, M. A.; Genevet, P.; Capasso, F. *Science* **2015**, *347*, 1342–1345.
- (30) Khorasaninejad, M.; Chen, W. T.; Devlin, R. C.; Oh, J.; Zhu, A. Y.; Capasso, F. *Science* **2016**, *352*, 1190–1194.
- (31) Maguid, E.; Yulevich, I.; Veksler, D.; Kleiner, V.; Brongersma, M. L.; Hasman, E. *Science* **2016**, *352*, 1202–1206.
- (32) Chen, S.; Cai, Y.; Li, G.; Zhang, S.; Cheah, K. W. *Laser & Photon. Rev.* **2016**, *10*, 322–326.
- (33) Pancharatnam, S. *Proc. Indian Acad. Sci. Sect. A* **1956**, *44*, 247–262.
- (34) Berry, M. V. *Proc. R. Soc. London, Ser. A* **1984**, *392*, 45–57.
- (35) Bomzon, Z.; Biener, G.; Kleiner, V.; Hasman, E. *Opt. Lett.* **2002**, *27*, 1141–1143.
- (36) Fleischer, A.; Kfir, O.; Diskin, T.; Sidorenko, P.; Cohen, O. *Nat. Photonics* **2014**, *8*, 543–549.
- (37) Chen, S. M.; Li, G. X.; Zeuner, F.; Wong, W. H.; Pun, E. Y. B.; Zentgraf, T.; Cheah, K. W.; Zhang, S. *Phys. Rev. Lett.* **2014**, *113*, 033901.
- (38) Konishi, K.; Higuchi, T.; Li, J.; Larsson, J.; Ishii, S.; Kuwata-Gonokami, M. *Phys. Rev. Lett.* **2014**, *112*, 135502.
- (39) Li, G.; Chen, S. M.; Pholchai, N.; Reineke, B.; Wong, P. W. H.; Pun, E. Y. B.; Cheah, K. W.; Zentgraf, T.; Zhang, S. *Nat. Mater.* **2015**, *14*, 607–612.
- (40) Tymchenko, M.; Gomez-Diaz, J. S.; Lee, J.; Nookala, N.; Belkin, M. A.; Alù, A. *Phys. Rev. Lett.* **2015**, *115*, 207403.
- (41) Ye, W.; Zeuner, F.; Li, X.; Reineke, B.; He, S.; Qiu, C. W.; Liu, J.; Wang, Y.; Zhang, S.; Zentgraf, T. *Nat. Commun.* **2016**, *7*, 11930.
- (42) Courtial, J.; Dholakia, K.; Allen, L.; Padgett, M. J. *Phys. Rev. A: At., Mol., Opt. Phys.* **1997**, *56*, 4193.
- (43) Zurch, M.; Kern, C.; Hansinger, P.; Dreischuh, A.; Spielmann, C. *Nat. Phys.* **2012**, *8*, 743–746.
- (44) Bloch, N. V.; Shemer, K.; Shapira, A.; Shiloh, R.; Juwiler, I.; Arie, A. *Phys. Rev. Lett.* **2012**, *108*, 233902.
- (45) Li, G.; Chen, S.; Cai, Y.; Zhang, S.; Cheah, K. W. *Adv. Opt. Mater.* **2014**, *2*, 389–393.
- (46) Keren-Zur, S.; Avayu, O.; Michaeli, L.; Ellenbogen, T. *ACS Photonics* **2016**, *3*, 117–123.
- (47) Almeida, E.; Shalem, G.; Prior, Y. *Nat. Commun.* **2016**, *7*, 10367.
- (48) Segal, N.; Keren-Zur, S.; Hendler, N.; Ellenbogen, T. *Nat. Photonics* **2015**, *9*, 180–184.
- (49) Li, G.; Zentgraf, T.; Zhang, S. *Nat. Phys.* **2016**, *12*, 736–740.
- (50) O'Brien, K.; Suchowski, H.; Rho, J.; Salandrino, A.; Kante, B.; Yin, X.; Zhang, X. *Nat. Mater.* **2015**, *14*, 379–383.
- (51) Lee, J.; Tymchenko, M.; Argyropoulos, C.; Chen, P. Y.; Lu, F.; Demmerle, F.; Boehm, G.; Amann, M. C.; Alù, A.; Belkin, M. A. *Nature* **2014**, *511*, 65–69.